DOI: 10.1016/S1872-5813(23)60377-9

Effect of Fe_2O_3 on $ZrTiO_4$ support for NH_3-SCR catalytic performance

YUAN Long-teng[1,3], HU Ping[1,2,3,*], HU Bo-liang[1,2,*], HAN Jia-yu[1,2], MA Sheng-jie[1,3], YANG Fan[1,2], Alex A. Volinsky[4]

(1. *National and Local Joint Engineering Research Functional Center for Materials Processing*, *Xi'an University of Architecture and Technology*, *Xi'an* 710055, *China*;
2. *School of Metallurgy Engineering*, *Xi'an University of Architecture and Technology*, *Xi'an* 710055, *China*;
3. *School of Mechanical and Electrical Engineering*, *Xi'an University of Architecture and Technology*, *Xi'an* 710055, *China*;
4. *Department of Mechanical Engineering*, *University of South Florida*, 4202 *E. Fowler Ave.*, *ENG* 030, *Tampa*, *FL* 33620, *USA*)

Abstract: The selective catalytic reduction (SCR) NH_3 catalyst is mainly used in industrial production and automobile exhaust cleaning. In this study, a novel α% Fe_2O_3/$ZrTiO_4$ (α=0%, 8%, 12%, 15%) catalyst was prepared by the coprecipitation impregnation method. The results show that the NO_x conversion rate of 12% Fe_2O_3/$ZrTiO_4$ catalyst with the optimal composition is high above 80% at 250−400 °C, close to 100% at 300 °C, and N_2 selectivity is high above 90% at 200−450 °C. The redox properties, surface acidity, and $O_\beta/(O_\alpha + O_\beta)$ ratio of $ZrTiO_4$ catalysts are improved after loading Fe_2O_3 on the $ZrTiO_4$ surface, which is attributed not only to the porous structure of α% Fe_2O_3/$ZrTiO_4$ catalyst but also to the synergistic interaction between the active component Fe_2O_3 and the support $ZrTiO_4$. In addition, in-situ DRIFT reactions show that the NH_3-SCR reaction of 12% Fe_2O_3/$ZrTiO_4$ catalyst follows the Eley-Rideal mechanism. A clear reaction mechanism is conducive to a deeper understanding of the reaction process of NO_x conversion during SCR. This work provides a feasible strategy for Fe-based SCR catalysts to replace V-based catalysts in the medium temperature range in the future.

Key words: Fe_2O_3/$ZrTiO_4$ catalyst; NH_3-SCR; Porous structure; Reaction mechanism.
CLC number: O643.36 **Document code:** A

In recent years, with the rapid development of science and technology, the smoke pollution produced by industrial power plants and automobile exhaust becomes more serious, and the pollutants emitted mainly include CO, C_xH_y, NO_x, and SO_2[1,2]. Among them, NO_x, as one of the main sources of air pollution, can cause photochemical smog, acid rain, and the greenhouse effect. At the same time, as a pollution gas, it can damage the human central nervous system and bring great pressure on human health and environmental preservation[3,4]. Therefore, effectively solving this problem can better balance the development between human beings and environmental protection.

So far, the commonly used flue gas deNO_x technologies include a selective catalytic reduction (SCR) and selective non-catalytic reduction (SNCR). The catalysts used in selective catalytic reduction mainly include noble metal catalysts, metal oxide catalysts, and molecular sieve catalysts. At present, a more mature metal oxide V_2O_5-$WO_3(MoO_3)$/TiO_2 catalyst is used commercially with a temperature range between 300 and 400 °C, high NO_x conversion rate, excellent stability, and performance[5,6]. However, the vanadium system has a narrow operating temperature window, low activity at low temperatures, high operating temperature (350−450 °C), and vanadium toxicity[7,8]. Therefore, it is important to develop a new catalyst system.

As an eco-friendly oxide, Fe_2O_3 has been widely used in NH_3-SCR reactions due to its low cost and the unsaturated properties of *d* orbitals[9]. In addition, the coupling between Fe^{3+} and Fe^{2+} also greatly enhanced the SCR activity[9]. The NO_x conversion rate of the $Fe_{1.2}Al_{0.8}O_x$ catalyst prepared by Bie et al.[10] is greater than 80% between 250 and 350 °C. The 3% Fe/WO_3-ZrO_2 catalyst prepared by the impregnation method of Foo et al.[11] achieved 80%−85% NO_x conversion at 400−550 °C. In addition, Fe_2O_3 as active components, such as Fe_2O_3/ZrO_2[12] and Fe_1-V_1/TiO_2[13], showed excellent SCR activity. However, the deNO_x efficiency of pure Fe_2O_3 in practical applications is still challenging.

There have been many studies of ZrO_2 and TiO_2 as catalyst carriers. TiO_2 carriers have good water resistance, trace SO_2 resistance, and high activity in NO

Received: 2023-03-15; Revised: 2023-04-08

* Corresponding author. E-mail: huping1985@126.com, huboliang@xauat.edu.cn.

本文的英文电子版由 Elsevier 出版社在 ScienceDirect 上出版 (http://www.sciencedirect.com/science/journal/18725813)

selection reduction in the NO-NH_3-O_2 system[14]. ZrO_2 carrier has good chemical stability, unique weak acid, and weak base dual function properties[15]. It is also a p-type semiconductor, and can easily produce oxygen holes, producing strong interactions with active components. However, Liu et al.[16] found that the BET surface area was often too low when ZrO_2 was used as a carrier alone. Guo et al.[17] found that the electron absorption ability of bulk TiO_2 support was not strong enough. In addition, ZrO_2 has three kinds of crystal phase structures (tetragonal, monoclinic, and cubic) and TiO_2 has two kinds of crystal phase structures (anatase and rutile). In the process of using the catalyst, ZrO_2 and TiO_2 as the carrier will undergo crystal phase changes, which will affect the reaction performance of the catalyst. Compared to a single oxide, we synthesized two metal oxides to prepare a $ZrTiO_4$ carrier with a high BET surface area and excellent thermal stability.

In this study, the α% Fe_2O_3/$ZrTiO_4$ catalyst was prepared by coprecipitation and impregnation methods, and its deNO_x activity was evaluated in a fixed-bed reactor. The physicochemical properties of the catalyst were characterized by X-ray diffraction (XRD), X-ray photoelectron spectroscopy (XPS), scanning electron microscopy (SEM), H_2 temperature-programmed reduction (H_2-TPR), NH_3 temperature-programmed desorption (NH_3-TPD), and N_2 physisorption. The reaction mechanism of the α% Fe_2O_3/$ZrTiO_4$ catalyst was further analyzed by *in-situ* diffuse reflectance infrared Fourier transform (DRIFT).

1 Experimental

1.1 Catalyst preparation

All chemicals used in the experiments, $Ti(SO_4)_2$ (Sinopharmed Chemical Reagent Co., LTD.) and $ZrOCl_2{\cdot}8H_2O$ (Shanghai Zhanyun Chemical Co., LTD.), were of analytical grade. During the experiment, 42.6% $Ti(SO_4)_2$ and 57.4% $ZrOCl_2{\cdot}8H_2O$ were dissolved in 200 mL deionized water and stirred. In the two precursors, ammonia was added to adjust the solution pH to 9 at room temperature, and the impurity ions were removed after filtration by deionized water for 6 times and by alcohol for another 3 times. $ZrTiO_4$ samples were prepared by drying and grinding at 80 °C and annealing at 500 °C for 80 min in the air atmosphere.

Different amounts of α% Fe_2O_3 in $Fe(NO_3)_3{\cdot}9H_2O$ (Macklin) were fully dissolved in deionized water, and then a certain amount of $ZrTiO_4$ powder was fully impregnated in $Fe(NO_3)_3$ aqueous solution, and stirred at room temperature for a period of time. First, the catalyst was dried at 80 °C for 10 h in air, and then dried at 110 °C for 12 h in vacuum. After grinding, the catalyst was annealed at 500 °C for 3 h. After natural cooling to room temperature, the calcined mixture was pressed, grinded and sieved to obtain α% Fe_2O_3/$ZrTiO_4$ catalyst, where α=0%, 8%, 12%, and 15%.

1.2 Catalyst characterization

Field emission scanning electron microscopy (FESEM, Gemini SEM 300) was used to observe the morphology of the catalyst and energy dispersive spectroscopy (EDX) was used to observe the distribution of Fe on the surface of $ZrTiO_4$. The phase composition was measured by powder XRD (Bruker AXS D8). The surface area of the catalyst was measured by the JW-BK222 instrument, and was calculated by the Brunauer-Emmett-Teller (BET) method. XPS characterization was performed using a Thermo ESCALAB 250XI instrument. The voltage was 16 kV, and the charge calibration was performed by using C 1*s*=284.8 eV as the standard. NH_3-TPD and H_2-TPR were carried out on a chemisorption analyzer US-Micromeritics-AutoChem II 2920 equipped with a thermal conductivity detector (TCD). For the H_2-TPR test, 140 mg samples were pretreated in 50 mL/min N_2 atmosphere at 400 °C for 60 min and then the temperature was reduced to 50 °C. Finally, the pretreated samples were analyzed in 5% H_2/He, 50 mL/min at 750 °C with a heating rate of 10 °C/min. In addition, for NH_3-TPD, 140 mg samples were pretreated in an N_2 atmosphere (30 mL/min) at 400 °C for 60 min and then the temperature was reduced to 50 °C. The pretreated samples were adsorbed in 1% NH_3/N_2 at 50 °C and then purged with N_2 for 60 min. The samples were heated from 50 to 750 °C (10 °C/min) at 50 mL/min in an N_2 atmosphere. The *in-situ* DRIFT spectra were obtained using a Thermo Scientific Nicolet 6700 spectrometer. The reaction conditions were as follows: 5.0×10^{-4} NH_3, 5.0×10^{-4} NO, 3% O_2 balanced by N_2, and the gas flow rate was 100 mL/min.

1.3 Catalytic activity test

The activity test was carried out in a fixed-bed quartz reactor with 0.8 g catalyst, crushed, and sieved to a 40−60 mesh range in a quartz tube. The inner diameter of quartz tube is 4.8 mm, and the length of catalytic bed is 8 cm. The test conditions were 5.0×10^{-4} NH_3, 5.0×10^{-4} NO, 3% O_2 balanced by N_2. The gas flow

rate was 500 mL/min, and the weight hourly space velocity (WHSV) was 37,500 mL/(g·h). The catalyst was pretreated in N_2 at 200 °C for 60 min. The test temperature was 100−500 °C. The outlet gas concentration of NO, NO_2, NH_3 and N_2O was measured by Thermo Scientific Nicolet 50 with DTGS detector. The NO_x conversion, N_2 selectivity and NH_3 conversion rate were calculated as:

$$NO_x\text{conversion}(\%) = \left(\frac{([NO]_{(in)}+[NO_2]_{(in)})-([NO]_{(out)}+[NO_2]_{(out)})}{[NO]_{(in)}+[NO_2]_{(in)}}\right)\times 100\% \quad (1)$$

$$N_2\text{ selectivity}(\%) = \left(1-\frac{2N_2O_{x(out)}}{NO_{x(in)}-NO_{x(out)}}\right)\times 100\% \quad (2)$$

$$NH_3\text{ conversion}(\%) = \left(\frac{[NH_3]_{(in)}-[NH_3]_{(out)}}{[NH_3]_{(in)}}\right)\times 100\% \quad (3)$$

2　Results and discussion

2.1　Morphology of α% Fe_2O_3/$ZrTiO_4$ catalyst

In order to analyze the surface characteristics of the samples, SEM characterization was carried out. As seen in Figure 1(a), the $ZrTiO_4$ particles exhibit irregular morphology and a fluffy porous structure on the sample surface. This fluffy multi-pore sample can promote the reaction gas to enter the mass transfer channel better, which is conducive to the adsorption and diffusion of the gas, and promote the catalytic performance of the catalyst[18]. After loading Fe_2O_3 on the surface of the $ZrTiO_4$ sample, it is found that α% Fe_2O_3/$ZrTiO_4$ and $ZrTiO_4$ samples show the same morphological characteristics, with a large number of pores on the surface, indicating that the loading of Fe_2O_3 does not affect the morphology of pure $ZrTiO_4$ (Figure 1 (b)). However, with the increase of Fe_2O_3 loading, the surface morphology of the catalyst became slightly rougher, possibly because of the aggregation of Fe_2O_3 on the surface of $ZrTiO_4$ support (Figure 1(c)&(d)).

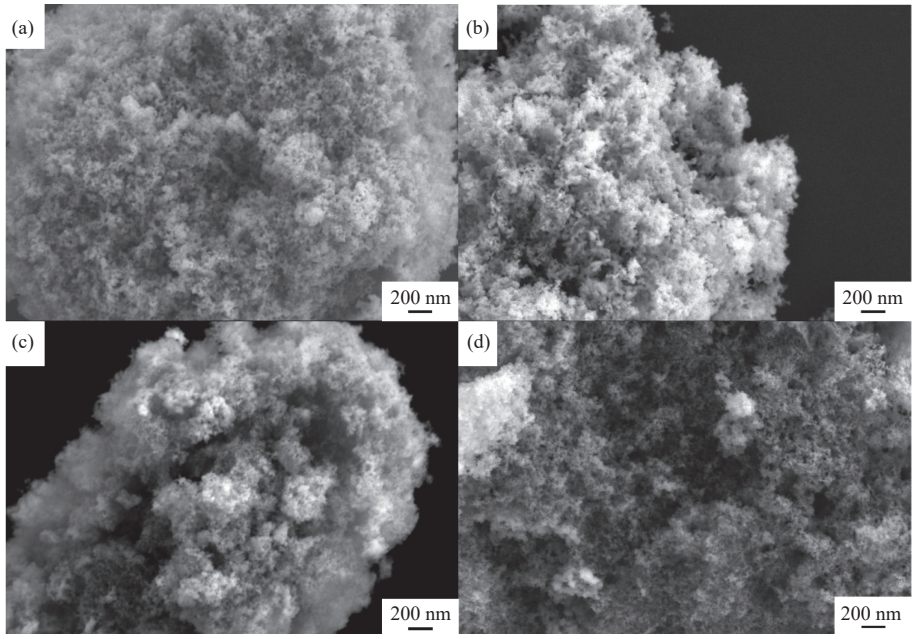

Figure 1　SEM images of $ZrTiO_4$ and α% Fe_2O_3/$ZrTiO_4$ samples
(a) $ZrTiO_4$; (b) 8% Fe_2O_3/$ZrTiO_4$; (c) 12% Fe_2O_3/$ZrTiO_4$; (d) 15% Fe_2O_3/$ZrTiO_4$

2.2　N_2 physisorption of α% Fe_2O_3/$ZrTiO_4$ catalyst

To further characterize the porous properties of the samples, N_2 adsorption-desorption was performed to obtain BET surface area, pore volume and pore size of the $ZrTiO_4$ and α% Fe_2O_3/$ZrTiO_4$ samples. The adsorption isotherms of the four samples are shown in Figure 2. All four curves have similar shapes and a hysteresis loop, which are typical type IV isotherms belonging to mesoporous structures with 2−50 nm pore sizes[19]. The BET surface area and pore size were further analyzed. Table 1 shows that the maximum specific surface area and pore volume of pure $ZrTiO_4$ are 161.3 m^2/g and 0.85 cm^3/g, and the specific surface area will be reduced to a certain extent after Fe_2O_3 is loaded on the surface. This may be because that Fe_2O_3 deposition blocks the pore channels of some $ZrTiO_4$

samples. With the increase of Fe_2O_3 loading, the specific surface area of α% Fe_2O_3/$ZrTiO_4$ catalyst decreases first, then increases, then decreases again, and the pore volume and pore size change correspondingly. This may be attributed to the fact that the deposited Fe_2O_3 will block the pores of $ZrTiO_4$, resulting in the decrease of the specific surface area and pore volume of the catalyst. Therefore, an appropriate amount of Fe_2O_3 is conducive to the interaction between the active components and the support. Among the composite catalysts, 12% Fe_2O_3/$ZrTiO_4$ catalyst has the largest specific surface area and pore volume, which are 139.6 m^2/g and 0.77 cm^3/g, respectively. Generally speaking, the higher the specific surface area of the catalyst, the more active sites will be provided for the SCR reaction, which in turn facilitates the adsorption of reaction gases such as NH_3 and NO_x[20]. Therefore, this is one of the key conditions for the 12% Fe_2O_3/$ZrTiO_4$ catalyst to have the highest SCR activity.

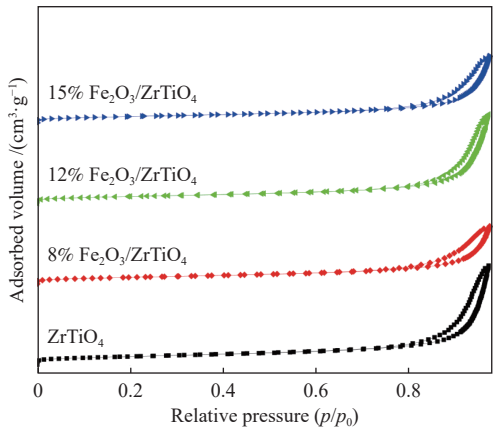

Figure 2 Adsorption isotherms of $ZrTiO_4$ and α% Fe_2O_3/$ZrTiO_4$ samples. the curves are offset for clarity and are plotted with the same y scale

Table 1 S_{BET} surface area, pore volume and pore size of $ZrTiO_4$ and α% Fe_2O_3/$ZrTiO_4$ samples

Sample	Surface area / ($m^2 \cdot g^{-1}$)	Pore volume / ($cm^3 \cdot g^{-1}$)	Pore size / nm
$ZrTiO_4$	161.3	0.85	21.19
8% Fe_2O_3/$ZrTiO_4$	134.3	0.50	14.87
12% Fe_2O_3/$ZrTiO_4$	139.6	0.77	22.02
15% Fe_2O_3/$ZrTiO_4$	129.1	0.58	17.92

2.3 Phases and energy spectra of α% Fe_2O_3/$ZrTiO_4$ catalyst

Figure 3 shows the XRD patterns of the $ZrTiO_4$ and α% Fe_2O_3/$ZrTiO_4$ samples. As seen in Figure 3, the XRD results of pure $ZrTiO_4$ samples show only the corresponding $ZrTiO_4$ reflections, which are in good agreement with the standard PDF card of $ZrTiO_4$ (PDF#74-1504). After loading Fe_2O_3 on the surface of $ZrTiO_4$, only the corresponding $ZrTiO_4$ XRD reflections are observed in α% Fe_2O_3/$ZrTiO_4$ catalyst, but no corresponding XRD reflections of Fe_2O_3 are observed, indicating that the doped Fe_2O_3 is highly dispersed on the surface of $ZrTiO_4$. Good dispersion can promote the interaction between the active components and the support, and improve the SCR activity of the catalyst[21]. In addition, the loading of Fe_2O_3 also reduces the reflection intensity of $ZrTiO_4$, and the crystallinity decreases significantly. Some diffraction reflections disappear completely because of the loading of Fe_2O_3, which enhances the amorphous form of $ZrTiO_4$. The results show that the doping of Fe_2O_3 promotes the interaction between the active components and the support.

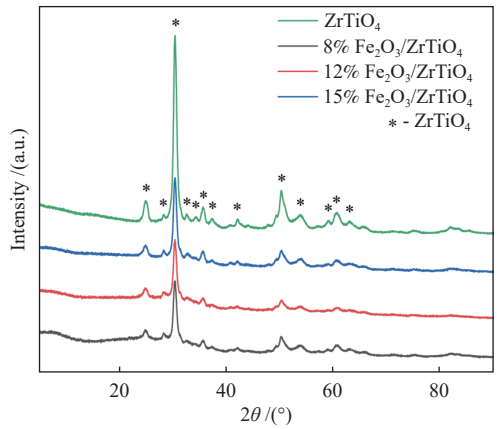

Figure 3 XRD patterns of $ZrTiO_4$ and α% Fe_2O_3/$ZrTiO_4$ samples

In order to further determine the dispersion state of the Fe element, the distribution of the Fe element on the surface of $ZrTiO_4$ support was characterized by EDX. As seen in Figure 4, there is a homogeneous distribution of Fe on the surface of $ZrTiO_4$ support, which is conducive to the SCR reaction of the catalyst. From the comparison of intensity, the contrast of Zr and Ti components is strong, while the contrast of Fe components is weak, because the molar percentage of Fe is only 12%, and its content is low.

2.4 Surface acidity of α% Fe_2O_3/$ZrTiO_4$ catalyst

The concentration of acid sites on the catalyst surface were tested by NH_3-TPD, and the results are shown in Figure 5. The first peak corresponds to the physically adsorbed NH_3 molecule at the weak acid site, the second peak corresponds to the chemically

adsorbed NH_3 at the weak acid site, and the third peak corresponds to the adsorbed NH_3 site at the strong acid site. Researchers generally believe that the chemically adsorbed NH_3 molecule can better participate in the SCR reaction[22]. Therefore, although all the samples have similar peaks and curves, it is obvious from Figure 5 that the peak areas of a weak acid, medium acid and strong acid of pure $ZrTiO_4$ are smaller than those of the composite $Fe_2O_3/ZrTiO_4$ catalyst, indicating that the Fe_2O_3 loading greatly increases the strength and number of acid sites of the catalyst. In addition to the acidity of Fe_2O_3, the Fe element enhances the interactions among Fe, Ti and Zr elements, and promotes the acidity of the catalyst surface. The relative curve area of the surface acidity of the four catalysts is 12% $Fe_2O_3/ZrTiO_4$ (1.41) > 15% $Fe_2O_3/ZrTiO_4$ (1.36) > 8% $Fe_2O_3/ZrTiO_4$ (1.28) > $ZrTiO_4$ (1). The 12% $Fe_2O_3/ZrTiO_4$ catalyst has the largest peak area and the lowest reduction peak in the medium and low-temperature region, which indicates that it has the highest surface acidity and more medium and weak acid sites, and can effectively adsorb more NH_3 molecules to promote the SCR performance of the catalyst[23].

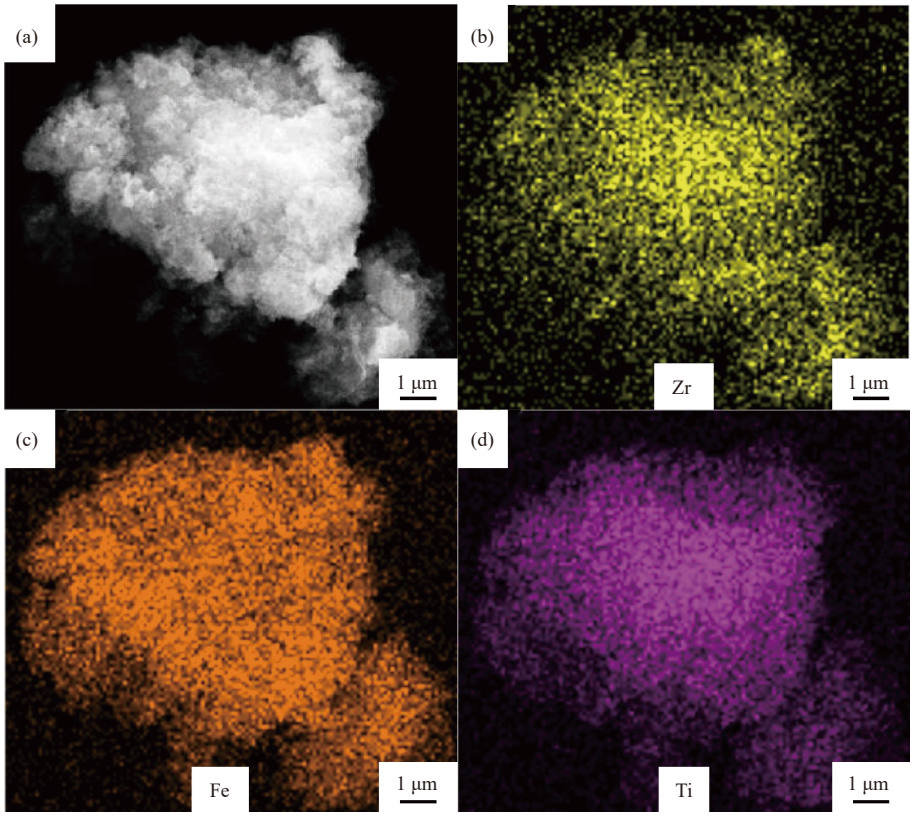

Figure 4 (a) SEM image and EDX elemental maps of the 12% $Fe_2O_3/ZrTiO_4$ catalyst: (b) Zr, (c) Fe, and (d) Ti

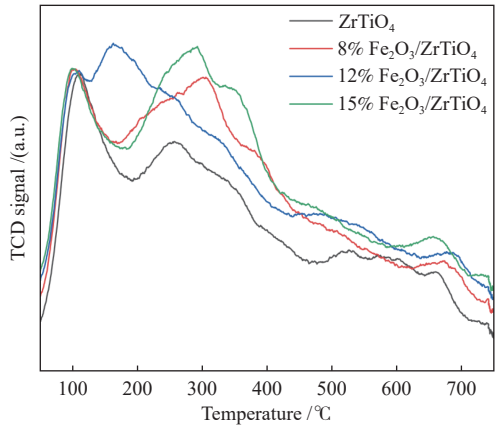

Figure 5 NH_3-TPD profiles of $ZrTiO_4$ and α% $Fe_2O_3/ZrTiO_4$ samples

2.5 Redox properties of α% $Fe_2O_3/ZrTiO_4$ catalyst

The redox properties of the catalyst and the interactions between the active components and the support were tested by H_2-TPR, and the results are shown in Figure 6. As can be seen in Figure 6, pure $ZrTiO_4$ has a single peak. Some studies claim that ZrO_2 has high thermal stability and is not easy to be reduced by H_2 below 900 °C[24], so this single peak may be attributed to the reduction of TiO_2 to Ti_2O_3. It is worth noting that after loading Fe_2O_3 on $ZrTiO_4$ support, three peaks can be seen in all α% $Fe_2O_3/ZrTiO_4$ catalysts, *i.e.* 342, 410 and 629 °C for 8% $Fe_2O_3/ZrTiO_4$ catalyst, 341, 430 and 646 °C for 12% $Fe_2O_3/ZrTiO_4$ catalyst,

354, 443 and 653 °C for 15% Fe_2O_3/$ZrTiO_4$ catalyst. The three peaks are attributed to Fe_2O_3→Fe_3O_4, TiO_2→Ti_2O_3 and Fe_3O_4→FeO, respectively. The relative curve area of the four catalysts consuming H_2 is 12% Fe_2O_3/$ZrTiO_4$ (3.27) > 15% Fe_2O_3/$ZrTiO_4$ (2.77) > 8% Fe_2O_3/$ZrTiO_4$ (1.48)>$ZrTiO_4$ (1). In α% Fe_2O_3/$ZrTiO_4$ catalyst, the new peak area increases and the reduction peak temperature decreases greatly, which means that the Fe_2O_3 loading improves the reduction performance of the Fe_2O_3/$ZrTiO_4$ catalyst. Therefore, the presence of Fe atoms affects the reduction performance of the Fe_2O_3/$ZrTiO_4$ catalyst, which may be attributed to the charge transfer between the Fe_2O_3 active component and the $ZrTiO_4$ support, resulting in a strong synergistic effect, leading to the electron transfer between the active component and the support, and finally promoting the SCR activity of the catalyst[25]. In addition, the 12% Fe_2O_3/$ZrTiO_4$ catalyst has the largest reduction peak area and the lowest reduction peak temperature, which indicate that it has the best reduction properties and thus has the best SCR activity, which is consistent with our test results.

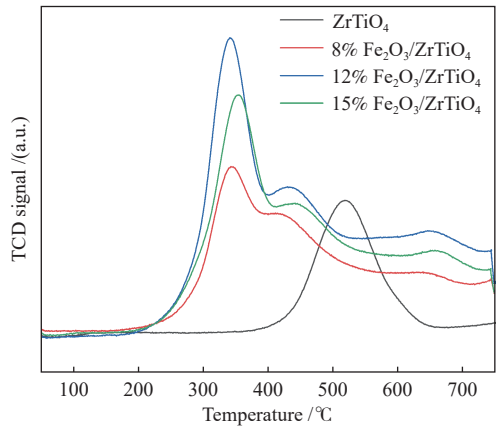

Figure 6 H_2-TPR profiles of $ZrTiO_4$ and α% Fe_2O_3/$ZrTiO_4$ samples

2.6 SCR activity of α% Fe_2O_3/$ZrTiO_4$ catalyst

Figure 7(a) shows the NH_3-SCR activity results of the four samples. It can be seen that the NO_x conversion rate of pure $ZrTiO_4$ samples increases continuously in the 100−500 °C range, but the maximum NO_x conversion rate is only 38.5% at 100−400 °C, and then the NO_x conversion rate can reach 86.3% at 500 °C because the reducing ability of $ZrTiO_4$ carrier is not active at low temperature. After loading Fe_2O_3 on the $ZrTiO_4$ carrier, the NO_x conversion rate is significantly increased. The NO_x conversion rate of α% Fe_2O_3/$ZrTiO_4$ samples is greater than 85% at 300−400 °C and greater than 95% at 300−350 °C. Then, as the temperature continues to rise, the NO_x conversion rate decreases significantly, mainly because the high oxidation ability of Fe_2O_3 makes NH_3 react with O_2, leading to the reduction of SCR activity. The NO_x conversion of the best 12% Fe_2O_3/$ZrTiO_4$ catalyst is greater than 80% at 250−400 °C and close to 100% at 300 °C, which is consistent with the H_2-TPR test results. The experimental results show that the loading of Fe_2O_3 can effectively improve the NH_3-SCR activity of the catalyst, which is attributed to the synergistic interaction between Fe, Zr and Ti elements to promote the electron transfer ability of the catalyst, which leads to the improvement of SCR activity. As shown in Figure 7(b), the N_2 selectivity of the four samples was further tested. The N_2 selectivity of pure $ZrTiO_4$ samples is less than 90% between 100 and 400 °C. However, after loading Fe_2O_3 on the surface of $ZrTiO_4$, the N_2 selectivity of α% Fe_2O_3/$ZrTiO_4$ samples is significantly improved, which is more than 90% at 200−450 °C, and then the N_2 conversion rate decreases slightly at 350 °C, which is similar to the NO_x conversion at high temperature. In addition, the results of NH_3 conversion during SCR reaction were also tested. As shown in Figure 7 (c), the NH_3 conversion rate of all samples continuously increases between 150 and 500 °C until it reaches 100%. However, above 300 °C, the NO_x conversion rate significantly decreases, while the NH_3 conversion rate continues to increase. In addition to the SCR reaction between NH_3 and NO in Eq. (4), the direct reaction between NH_3 and O_2 may occur due to the high oxidation capacity of Fe_2O_3 (Eq. (5), Eq. (6) and Eq. (7)), as shown in Figure 7(d). This is also confirmed by the decrease in NO conversion rate above 400 °C and the continuous increase of N_2O emission above 400 °C[26,27].

$$4NO + 4NH_3 + O_2 \rightarrow 4N_2 + 6H_2O \quad (4)$$

$$4NH_3 + 5O_2 \rightarrow 4NO + 6H_2O \quad (5)$$

$$2NH_3 + 2O_2 \rightarrow N_2O + 3H_2O \quad (6)$$

$$4NH_3 + 3O_2 \rightarrow 2N_2 + 6H_2O \quad (7)$$

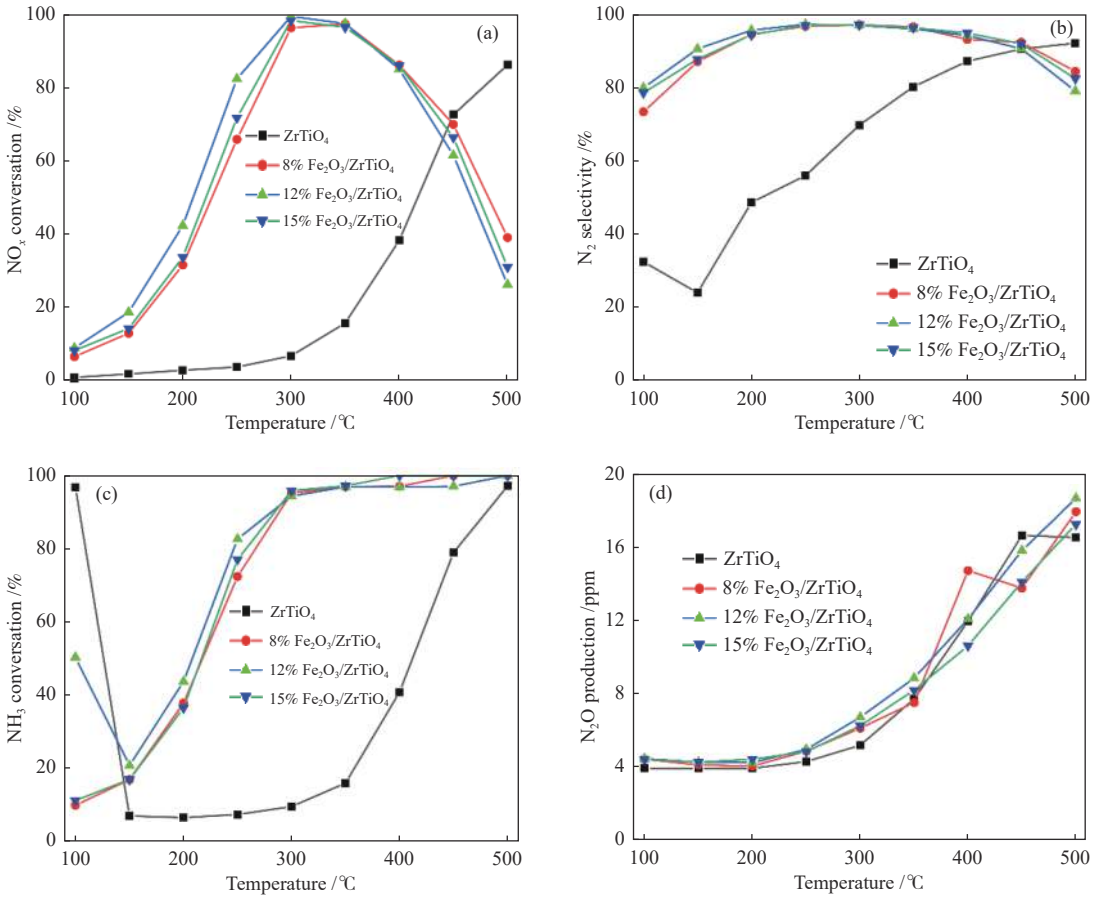

Figure 7　(a) NO_x conversion of $ZrTiO_4$ and α% $Fe_2O_3/ZrTiO_4$ samples; (b) N_2 selectivity; (c) NH_3 conversion; (d) N_2O emissions (Reactant feed contains 5.0×10^{-4} of NO, 6.0×10^{-4} of NH_3, 3% O_2, balanced with N_2)

2.7　Electron transport between Fe_2O_3 and $ZrTiO_4$ carrier

XPS was used to determine the content of elements on the catalyst surface, the state of metal oxides and the type of adsorbed oxygen, and to explore the interaction between the elements. Figure 8(a) shows the Zr 3*d* orbital XPS profiles of $ZrTiO_4$ and α% $Fe_2O_3/ZrTiO_4$ catalysts. The four catalysts all contain two typical characteristic peaks. The characteristic peak located at 182.37−182.47 eV is attributed to Zr^{4+} species, and the characteristic peak located at 184.67−184.87 eV is attributed to Zr $3d_{3/2}$. The Zr^{4+} binding energy of the four samples does not change significantly, indicating that the presence of Zr^{4+} in the catalyst is very stable, and the loading/calcination of Fe_2O_3 does not affect the stability of Zr^{4+}. In addition, the Zr^{4+} binding energy of the four catalysts is lower than the ZrO_2 standard of 182.7 eV, which proves the interaction between Zr and Ti[28]. As shown in Table 2, the content of Zr species decreases after loading 8% Fe_2O_3 on $ZrTiO_4$, but the content of Zr species remains almost unchanged when the loading of Fe_2O_3 is further increased, possibly because some Fe species exist in the bulk of ZrO_2.

Figure 8(b) shows the Ti 2*p* XPS profiles of $ZrTiO_4$ and α% $Fe_2O_3/ZrTiO_4$ catalysts. The characteristic peak at 458.47−458.67 eV belongs to Ti $2p_{3/2}$, and the peak at 464.17−464.47 eV belongs to Ti $2p_{1/2}$, indicating the existence of Ti^{4+}. The binding energy of pure $ZrTiO_4$ catalyst is 458.47 eV. The characteristic peak of α% $Fe_2O_3/ZrTiO_4$ catalyst after Fe_2O_3 deposition moves to a higher binding energy and increases with the Fe_2O_3 content, indicating that the electron density of the Ti element decreases. In addition, the shift of characteristic peaks indicates the presence of Fe_2O_3, which promotes the strong interaction between Ti and Fe, leading to the migration of electron clouds[29].

Figure 8(c) shows the Fe 2*p* XPS pattern of α% $Fe_2O_3/ZrTiO_4$ catalyst. The XPS pattern has a larger fold because of less Fe loading. The characteristic peaks located at 711 and 725 eV belong to Fe $2p_{3/2}$ and Fe $2p_{1/2}$ peaks, respectively[30]. Fe $2p_{3/2}$ is divided into Fe^{3+} (711.17−711.87 eV) and Fe^{2+} (709.27−710.67 eV)

sub-peaks, respectively[31]. As shown in Table 2, with the increase of Fe_2O_3 loading, the Fe content on the catalyst surface increases and the $Fe^{3+}/(Fe^{3+}+Fe^{2+})$ ratio increases continuously from 43% to 91.7%. This shows that there is electron transfer between Fe_2O_3 and the carrier, and some electrons from the carrier are transferred to Fe_2O_3. It can be speculated that there is a strong interaction between Fe, Ti and Zr, which leads to the coexistence of Fe in different valence states on the surface of the catalyst.

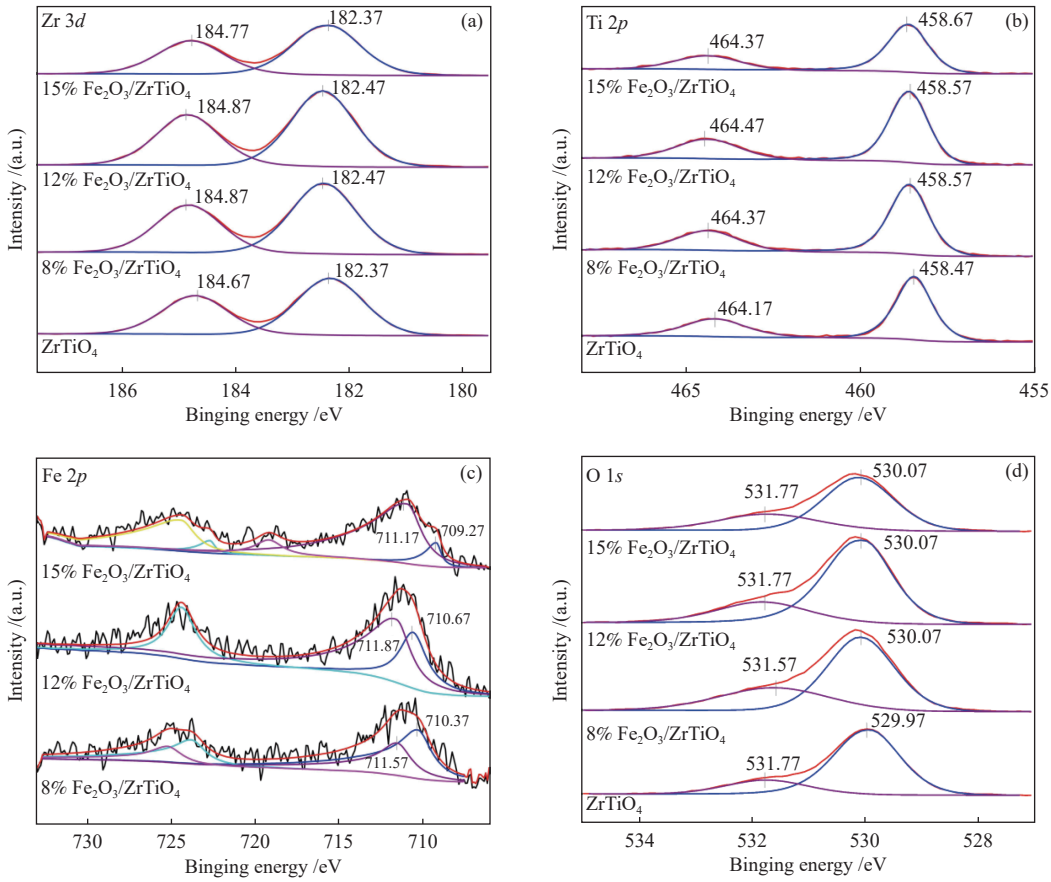

Figure 8 XPS profiles of $ZrTiO_4$ and α% $Fe_2O_3/ZrTiO_4$ samples: (a) Ti 2*p*; (b) Zr 3*d*; (c) Fe 2*p*; (d) O 1*s*

Table 2 XPS concentration of $ZrTiO_4$ and α% $Fe_2O_3/ZrTiO_4$

Sample	Atomic concentration				Relative concentration /%	
	Fe	Zr	Ti	O	$O_\beta/(O_\alpha+O_\beta)$	$Fe^{3+}/(Fe^{3+}+Fe^{2+})$
$ZrTiO_4$	–	14.4	15.3	70.3	23.1	–
8% $Fe_2O_3/ZrTiO_4$	1.85	13.3	13.2	71.6	34.0	43
12% $Fe_2O_3/ZrTiO_4$	2.21	13.3	12.8	71.6	31.7	73.4
15% $Fe_2O_3/ZrTiO_4$	2.68	13.2	13.1	71.0	28.7	91.7

As shown in Figure 8(d), the two characteristic peaks in the XPS pattern of the O 1*s* peak of $ZrTiO_4$ and α% $Fe_2O_3/ZrTiO_4$ catalysts are attributed to the lattice oxygen (O_α) at 530−531 eV, and the other characteristic peak at 531−532 eV is attributed to the surface chemisorbed oxygen (O_β)[32,33]. Generally, in SCR reaction, since the adsorbed oxygen is more active, it is easy to oxidize NO to NO_2, so it is easy to participate in the catalytic reaction[32]. As shown in Table 2, O atom concentration is the highest on the surface of all samples. The relative concentration of $O_\beta/(O_\alpha+O_\beta)$ in pure $ZrTiO_4$ catalyst is 23.1%. After Fe_2O_3 is loaded on the $ZrTiO_4$ catalyst, the relative concentration of oxygen adsorption on the surface of α% $Fe_2O_3/ZrTiO_4$ catalyst is higher than pure $ZrTiO_4$ catalyst. These results indicate that Fe loading enhances the chemisorption oxygen concentration of α% $Fe_2O_3/ZrTiO_4$ catalyst, and promotes the adsorption

of oxygen on the surface to participate in SCR reaction. This indicates that the strong interaction between Fe, Ti and Zr can induce surface active sites to activate oxygen. However, with the increase of Fe loading, the ratio of $O_\beta/(O_\alpha + O_\beta)$ decreased, which may be attributed to the formation of aggregates on the surface of $ZrTiO_4$ by Fe_2O_3 species.

2.8 Adsorption of NH_3(NO_x) species

It is of great significance to determine the reaction mechanism of 12% $Fe_2O_3/ZrTiO_4$ catalyst by studying the adsorption behavior of NH_3 and NO_x species by *in-situ* DRIFT. Figure 9(a) shows DRIFT spectra of adsorbed NH_3 species on a 12% $Fe_2O_3/ZrTiO_4$ catalyst surface. At 50 °C, a series of peaks appear in 12% $Fe_2O_3/ZrTiO_4$ catalysts stabilized by NH_3 adsorption. The adsorption peak at 984 cm^{-1} can be attributed to the gas phase or weakly adsorbed NH_3[34]. The adsorption peak at 1005 cm^{-1} is attributed to the gas phase or weakly adsorbed NH_3[34]. The adsorption peak at 1070 cm^{-1} is attributed to the coordinated NH_3 at the Lewis acid site[34,35]. The adsorption peak at 1244 cm^{-1} is attributed to the coordination of NH_3 at the Lewis acid site[34,36]. The adsorption peak at 1362 cm^{-1} is attributed to the wagging vibration of NH_2 species[37]. The adsorption peak at 1440 cm^{-1} is attributed to NH_4^+ species at the Brønsted acid site[38]. The adsorption peak at 1521 cm^{-1} is attributed to an amide (NH_2) substance[37]. The adsorption peaks at 2887 cm^{-1} and 2951 cm^{-1} are attributed to NH_4^+ species at the Brønsted acid site[38,39]. The adsorption peak at 3614 cm^{-1} is attributed to surface O−H/N−H stretching[40,41]. In addition, with the increase in temperature, the adsorbed NH_3 species on the surface of the catalyst changed, and the adsorption peaks at 984 and 1244 cm^{-1} continuously weakened, indicating that the adsorbed NH_3 species on the surface of 12% $Fe_2O_3/ZrTiO_4$ catalyst decreased. The above can be attributed to the desorption of adsorbed species at high temperatures. The adsorption peak at 1521 cm^{-1} constantly shifted to 1491 cm^{-1} with the increase in temperature, which may be because the unstable adsorption peak at 1521 cm^{-1} was transformed into more stable species. In addition, the adsorption peaks of 1005, 1070, 1362, 1440, 2887, 2951 and 3614 cm^{-1} on 12% $Fe_2O_3/ZrTiO_4$ catalysts do not change significantly with the increase of temperature, indicating that the adsorptions are relatively stable, which may be one of the reasons for the high activity of the 12% $Fe_2O_3/ZrTiO_4$ catalyst.

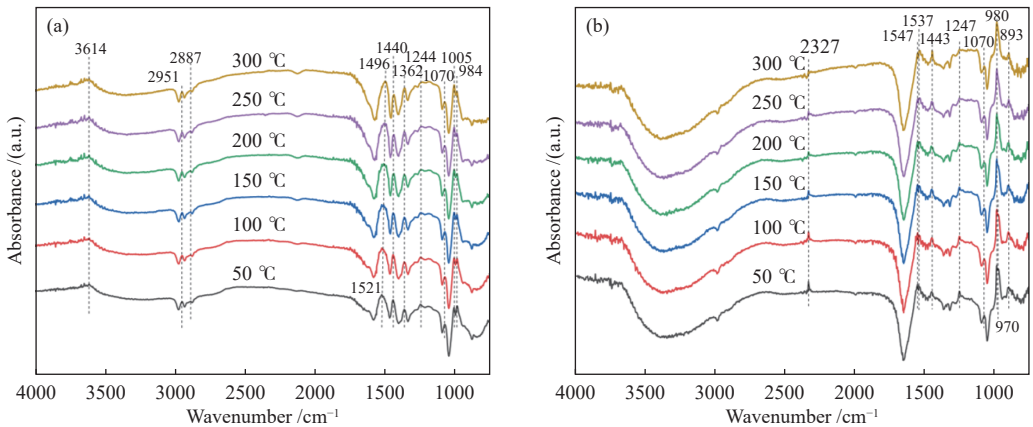

Figure 9　DRIFT spectra of (a) NH_3 adsorption and (b) NO + O_2 adsorption on 12% $Fe_2O_3/ZrTiO_4$ catalyst at different temperatures

Figure 9(b), shows DRIFT spectra of adsorbed NO_x species on the surface of a 12% $Fe_2O_3/ZrTiO_4$ catalyst. At 50 °C, a series of adsorption peaks appear after 12% $Fe_2O_3/ZrTiO_4$ catalyst adsorbs NO + O_2. The peaks at 970 and 980 cm^{-1} can be attributed to cis-$(N_2O_2)^{2-}$ species[42]. The adsorption peak at 1070 cm^{-1} is attributed to bidentate nitrate[43]. The adsorption peak at 1247 cm^{-1} is attributed to bridge nitrate[44,45]. The adsorption peak at 1443 cm^{-1} is attributed to nitro compounds[46]. The adsorption peaks at 1537 and 1547 cm^{-1} are attributed to bidentate nitrate[46,47]. The adsorption peak at 2327 cm^{-1} belongs to the adsorbed state N_2O[48]. The miscellaneous peaks above 3600 cm^{-1} are attributed to the surface basic hydroxyl band[48]. In addition, with the increase in temperature, some adsorption peaks changed significantly, and the adsorption peak located at 970 cm^{-1} disappeared when the temperature increased to 150 °C. The intensity of the adsorption peaks at 1247, 1547 and 2327 cm^{-1} decreases with temperature, which means that these adsorptions are not stable on the surface of the 12% $Fe_2O_3/ZrTiO_4$ catalyst.

2.9 Reaction mechanism of the 12% $Fe_2O_3/ZrTiO_4$ catalyst

Based on the previous conclusions of adsorption peaks of NH_3 species and NO_x species adsorbed by 12% $Fe_2O_3/ZrTiO_4$ catalyst at different temperatures, we further determined the reaction mechanism on 12% $Fe_2O_3/ZrTiO_4$ catalyst by pre-adsorbed NH_3 (NO + O_2) and then passing through NO + O_2 (NH_3). Because the 12% $Fe_2O_3/ZrTiO_4$ catalyst has the highest SCR activity at 300 °C, the SCR reaction mechanism on the surface of 12%$Fe_2O_3/ZrTiO_4$ catalyst was studied by selecting 300 °C as the in-situ DRIFT test temperature.

Figure 10(a), shows the in-situ DRIFTs spectra of 12% $Fe_2O_3/ZrTiO_4$ catalyst surface adsorbed NH_3 at 300 °C for 30 min before N_2 scavenging and blowing into NO + O_2. Figure 10(a) shows that a series of adsorption peaks appear on the surface of 12% $Fe_2O_3/ZrTiO_4$ catalyst after pre-adsorption of NH_3, and both ionic NH_4^+ species and coordinated NH_3 species appear on the surface of the catalyst. After the introduction of NO + O_2, some characteristic peaks changed significantly. With the increase of NO + O_2 penetration time, the adsorption peak at 950 cm^{-1} belonging to the gas phase or weakly adsorbed NH_3 began to weaken, and the intensity of the adsorption peak at 1765 cm^{-1} (NH_4^+) began to weaken, and no new adsorption peak appeared on the catalyst surface. This indicates that the NH_3 species adsorbed on the surface of the catalyst reacted with the NO_x species entering the catalyst. Then, NO + O_2 was pre-adsorbed on the surface of 12% $Fe_2O_3/ZrTiO_4$ catalyst at 300 °C for 30 min, and NH_3 was introduced after N_2 scavenging. As seen in Figure 10(b), NO adsorbed NO_x species are observed in DRIFT spectra after NO + O_2 gas is pre-adsorbed by the catalyst, which means that 12% $Fe_2O_3/ZrTiO_4$ catalyst does not adsorb NO_x species at 300 °C, and then after NH_3 is continuously introduced, new adsorption peaks (945, 1167, 1252, 1360, 1425, 1498 cm^{-1}) appeared at 3 min, and the intensity of the new adsorption peak also increased with the introduction of NH_3. The adsorption peaks of Lewis acid sites (1167, 1252 cm^{-1}) and Brønsted (1360, 1425, 1498 cm^{-1}) on the catalyst surface reached a stable state after the introduction of NH_3 for 60 min. Therefore, 12% $Fe_2O_3/ZrTiO_4$ catalyst in NH_3-SCR reaction is mainly through the Eley-Rideal (E-R) reaction mechanism, as shown in Eq. (8), (9) and (10). Gaseous NH_3 molecules adsorbed on the active site on the catalyst surface to form adsorbed NH_3 species, and then reacted directly with gaseous NO_x to generate adsorbed N_2, which is desorbed to produce final product N_2 (Figure 11).

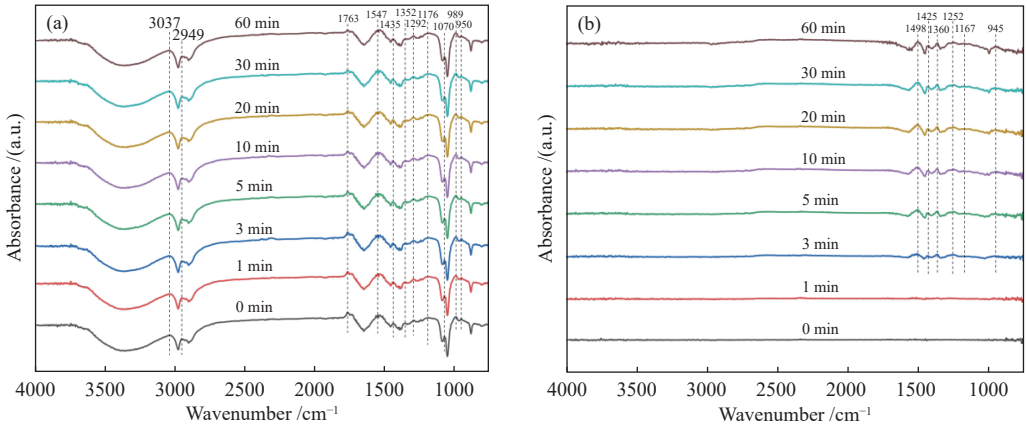

Figure 10 DRIFT spectra of reaction between (a) pre-adsorption of NH_3 and NO + O_2 (b) pre-adsorption of NO + O_2 and NH_3 on 12% $Fe_2O_3/ZrTiO_4$ catalyst

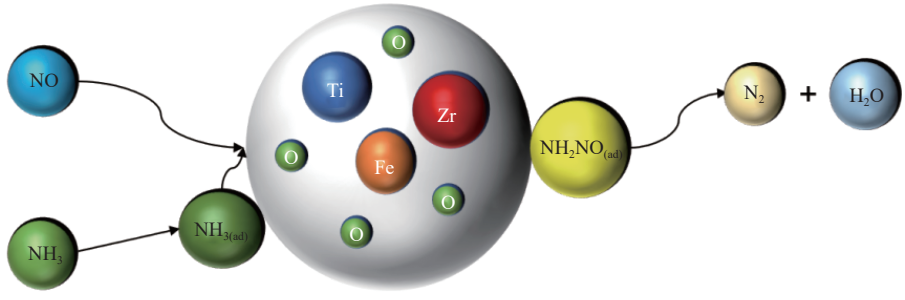

Figure 11 Reaction mechanism of 12% $Fe_2O_3/ZrTiO_4$ catalyst

$$NH_{3(g)} + * \rightarrow NH_{3(ads)} \quad (8)$$

$$NH_{3(ads)} + NO_{x(g)} \rightarrow NH_2NO_{(ads)} \quad (9)$$

$$NH_2NO_{(ads)} \rightarrow N_{2(g)} + H_2O \quad (10)$$

Note: * represents the active site on the catalyst; *g* represents the gas phase component; *ads* represents the adsorbed component.

3 Conclusions

Fe_2O_3 modified $ZrTiO_4$ composite oxide catalyst shows excellent NO_x conversion rate and N_2 selectivity. The best temperature window is between 250 and 400 °C, the NO_x conversion rate is greater than 80% and N_2 selectivity is greater than 90% at 200−450 °C.

The excellent SCR activity is mainly due to the synergistic interaction between Fe_2O_3 and $ZrTiO_4$ support, which leads to the best redox performance and surface acidity of the 12% $Fe_2O_3/ZrTiO_4$ catalyst. In addition, the presence of high surface area, high dispersion and the porous structure can also promote the ability of α% $Fe_2O_3/ZrTiO_4$ catalyst to adsorb NH_3 species, thus promoting the catalytic activity of the catalyst.

In-situ DRIFT shows that the surface of 12% $Fe_2O_3/ZrTiO_4$ catalyst mainly follows the E-R mechanism at 300 °C.

Acknowledgments

This work was supported by the Scientific and Technological Innovation Team Project of the Shaanxi Innovation Capability Support Plan, China (2022TD-30), the Youth Innovation Team of Shaanxi Universities (2019-2022), the top young talents project of "Special support program for high-level talents" in the Shaanxi Province (2018-2023), and the International Science and Technology Cooperation Program of the Shaanxi Province (2022KW-39), Xi'an Science and Technology Planning Project (2022JH-RYFW-0196).

References

[1] ROY B, CHOO W L, BHATTACHARYA S. Prediction of distribution of trace elements under Oxy-fuel combustion condition using Victorian brown coals[J]. Fuel, 2013, **114**: 135−142.

[2] GANESH C D, SUBHASHISH D, DEVENDRA M, RAM P. Study of Fe, Co, and Mn-based perovskite-type catalysts for the simultaneous control of soot and NOx from diesel engine exhaust[J]. Materials Discovery, 2017, **10**: 37−42.

[3] SEINFELD J H. Urban Air Pollution: State of the Science[J]. Science, 1989, **243**(4892): 745−752.

[4] LIU Z M, HAO J M, FU L X, ZHU T L. Study of Ag/La0.6Ce0.4CoO3 catalysts for direct decomposition and reduction of nitrogen oxides with propene in the presence of oxygen[J]. Applied Catalysis B:Environmental, 2003, **44**(4): 355−370.

[5] TOPSOE N Y. Mechanism of the selective catalytic reduction of nitric oxide by ammonia elucidated by in situ on-line fourier transform infrared spectroscopy[J]. Science (New York, N. Y.), 1994, **265**(5176): 1217−9.

[6] CHEN L, LI J H, GE M F. Promotional Effect of Ce-doped V2O5-WO3/TiO2 with Low Vanadium Loadings for Selective Catalytic Reduction of NOx by NH3[J]. The Journal of Physical Chemistry C, 2009, **113**(50): 21177−21184.

[7] LONG R Q, YANG R T. Superior Fe-ZSM-5 catalyst for selective catalytic reduction of nitric oxide by ammonia[J]. Journal of the American Chemical Society, 1999, **121**(23): 5595−5596.

[8] LIAN Z H, LIU F D, HE H. Enhanced Activity of Ti-Modified V2O5/CeO2 Catalyst for the Selective Catalytic Reduction of NOx with NH3[J]. Industrial & Engineering Chemistry Research, 2014, **53**(50): 19506−19511.

[9] HUANG T J, ZHANG Y P, ZHUANG K, LU BIN, ZHU YIWEN, SHEN KAI. Preparation of honeycombed holmium-modified Fe-Mn/TiO2 catalyst and its performance in the low temperature selective catalytic reduction of NOx[J]. Journal of Fuel Chemistry and Technology, 2018, **46**(3): 319−327.

[10] BIE X, WU K, JIAO K L, ZHAO K, CHEN X Y, MA SUANGCHEN. Behavior and structure tuning of (Mn&Fe)AlOx-based catalysts for superior denitrification performance[J]. Journal of Environmental Chemical Engineering, 2021, **9**(5): 106153.

[11] FOO R, VAZHNOVA T, LUKYANOV D B, MILLINGTON P, COLLIER J, RAJARAM R, GOLUNSKI S. Formation of reactive Lewis acid sites on Fe/WO3-ZrO2 catalysts for higher temperature SCR applications[J]. Applied Catalysis B-Environmental, 2015, **162**: 174−179.

[12] FAN B Y, ZHANG Z Y, LIU C X, LIU Q L. Investigation of Sulfated Iron-Based Catalysts with Different Sulfate Position for Selective Catalytic Reduction of NOx with NH3[J]. Catalysts, 2020, **10**(9): 1035.

[13] HUANG H F, CHEN Y J, YANG R, ZHU Q L, LU H F. Fe-V/TiO2 catalysts for selective catalytic reduction of NOx with NH3 in diesel exhaust[J]. Journal of Fuel Chemistry and Technology, 2014, **42**(6): 751−757.

[14] ZHOU Y Y, XIE Z Y, JIANG J X, WANG J, SONG X Y, HE Q, DING W, WEI Z D. Lattice-confined Ru clusters with high CO tolerance and activity for the hydrogen oxidation reaction (vol 3, pg 454, 2020)[J]. Nature Catalysis, 2021, **4**(4): 341−341.

[15] WEI X L, ZHAO R Q, CHU B X, XIE S Z, QIN Q J, CHEN K, LI L L, ZHAO S L, BIN LI, DONG L H. Significantly enhanced activity and SO2 resistance of Zr-modified CeTiOx catalyst for low-temperature NH3-SCR by H2 reduction treatment[J]. Molecular Catalysis, 2022, **518**: 112069.

[16] LIU C X, BI Y L, LI J H. Activity enhancement of sulphated Fe2O3 supported on TiO2–ZrO2 for the selective catalytic reduction of NO by NH3[J]. Applied Surface Science, 2020, **528**: 146695.

[17] GUO K, JI J W, OSUGA R, ZHU Y X, SUN J F, TANG C J, KONDO J N, DONG L. Construction of Fe2O3 loaded and mesopore confined thin-

layer titania catalyst for efficient NH3-SCR of NOx with enhanced H2O/SO2 tolerance[J]. Applied Catalysis B-Environmental, 2021, **287**: 119982.

[18] GONG Z Q, NIU S L, ZHANG Y J, LU C M. Facile synthesis of porous α-Fe2O3 nanostructures from MIL-100(Fe) via sacrificial templating method, as efficient catalysts for NH3-SCR reaction[J]. Materials Research Bulletin, 2020, **123**: 110693.

[19] FANG N J, GUO J X, SHU S, LUO H D, CHU Y H, LI J J. Enhancement of low-temperature activity and sulfur resistance of Fe0.3Mn0.5Zr0.2 catalyst for NO removal by NH3-SCR[J]. Chemical Engineering Journal, 2017, **325**: 114−123.

[20] LIU F D, SHAN W P, LIAN Z H, LIU J J, HE H. The smart surface modification of Fe2O3 by WOx for significantly promoting the selective catalytic reduction of NOx with NH3[J]. Applied Catalysis B:Environmental, 2018, **230**: 165−176.

[21] ZHAO K, MENG J P, LU J Y, HE Y, HUANG H Z, TANG Z C, ZHEN X P. Sol-gel one-pot synthesis of efficient and environmentally friendly iron-based catalysts for NH3-SCR[J]. Applied Surface Science, 2018, **445**: 454−461.

[22] HOU Y Q, WANG J C, LI Q Y, LIU Y J, BAI Y R, ZENG Z Q, HUANG Z G. Environmental-friendly production of FeNbTi catalyst with significant enhancement in SCR activity and SO2 resistance for NOx removal[J]. Fuel, 2021, **285**: 119133.

[23] REN D D, GUI K T, GU S C, WEI Y L. Mechanism of improving the SCR NO removal activity of Fe2O3 catalyst by doping Mn[J]. Journal of Alloys and Compounds, 2021, **867**: 158787.

[24] SHEN B X, WANG Y Y, WANG F M, LIU T. The effect of Ce-Zr on NH3-SCR activity over MnOx(0.6)/Ce0.5Zr0.5O2 at low temperature[J]. Chemical Engineering Journal, 2014, **236**: 171−180.

[25] SWIRK K, WANG Y, HU C W, LI L, DA C P, DELAHAY G. Novel Preparation of Cu and Fe Zirconia Supported Catalysts for Selective Catalytic Reduction of NO with NH3[J]. Catalysts, 2021, **11**(1): 55.

[26] LI C X, XIONG Z B, HE J F, QU X K, LI Z Z, NING X, LU W, WU S M, Tan L Z. Influence of ignition atmosphere on the structural properties of magnetic iron oxides synthesized via solution combustion and the NH3-SCR activity of W/Fe2O3 catalyst[J]. Applied Catalysis a-General, 2020, **602**: 117726.

[27] LI Y F, HOU Y Q, ZHANG Y Z, YANG Y T, HUANG Z G. Confinement of MnOx@Fe2O3 core-shell catalyst with titania nanotubes: Enhanced N2 selectivity and SO2 tolerance in NH3- SCR process[J]. Journal of colloid and interface science, 2021, **608**: 2224−2234.

[28] ZHOU X, YU F, SUN R B, TIAN J Q, WANG Q, DAI B, DAN J M, PFEIFFER Heriberto. Two-dimensional MnFeCo layered double oxide as catalyst for enhanced selective catalytic reduction of NOx with NH3 at low temperature (25-150 degrees C)[J]. Applied Catalysis a-General, 2020, **592**: 117432.

[29] SONG L, MA K, TIAN W, JI J Y, LIU C J, TANG S Y, JIANG W, YUE H R, LIANG B. An environmentally friendly FeTiSOx catalyst with a broad operation-temperature window for the NH3-SCR of NOx[J]. Aiche Journal, 2019, **65**(10): e16684.

[30] XU L T, NIU S L, LU C M, ZHANG Q, LI J. Influence of calcination temperature on Fe0.8Mg0.2Oz catalyst for selective catalytic reduction of NOx with NH3[J]. Fuel, 2018, **219**: 248−258.

[31] WANG X B, ZHANG L, WU S G, ZOU W X, YU S H, SHAO Y, DONG L. Promotional Effect of Ce on Iron-Based Catalysts for Selective Catalytic Reduction of NO with NH3[J]. Catalysts, 2016, **6**(8): 112.

[32] XIONG Z B, WU C, HU Q, WANG Y Z, JIN J, LU C M, GUO D X. Promotional effect of microwave hydrothermal treatment on the low-temperature NH3-SCR activity over iron-based catalyst[J]. Chemical Engineering Journal, 2016, **286**: 459−466.

[33] ZHOU Y H, REN S, WANG M M, YANG J, CHEN Z C, CHEN L. Mn and Fe oxides co-effect on nanopolyhedron CeO2 catalyst for NH3-SCR of NO[J]. Journal of the Energy Institute, 2021, **99**: 97−104.

[34] WU Z B, JIANG B Q, LIU Y, WANG H Q, JIN R B. DRIFT study of manganese/ titania-based catalysts for low-temperature selective catalytic reduction of NO with NH3[J]. Environmental science & technology, 2007, **41**(16): 5812−7.

[35] GUAN B, LIN H, ZHU L, HUANG Z. Selective Catalytic Reduction of NOx with NH3 over Mn, Ce Substitution Ti0.9V0.1O2-delta Nanocomposites Catalysts Prepared by Self-Propagating High-Temperature Synthesis Method[J]. Journal of Physical Chemistry C, 2011, **115**(26): 12850−12863.

[36] JIANG B Q, LI Z G, LEE S C. Mechanism study of the promotional effect of O-2 on low-temperature SCR reaction on Fe-Mn/TiO2 by DRIFT[J]. Chemical Engineering Journal, 2013, **225**: 52−58.

[37] LI X Y, CHEN J, LU C M, LUO G Q, YAO H. Performance of Mo modified γ-Fe2O3 catalyst for selective catalytic reduction of NOx with ammonia: Presence of arsenic in flue gas[J]. Fuel, 2021, **294**: 120552.

[38] CHEN L, LI J H, GE M F. DRIFT study on cerium-tungsten/titania catalyst for selective catalytic reduction of NOx with NH3[J]. Environmental science & technology, 2010, **44**(24): 9590−6.

[39] HADJIIVANOV K I. Identification of Neutral and Charged N x O y Surface Species by IR Spectroscopy[J]. Catalysis Reviews, 2000, **42**(1-2): 71−144.

[40] LIU F D, HE H, DING Y, ZHANG C B. Effect of manganese substitution on the structure and activity of iron titanate catalyst for the selective catalytic reduction of NO with NH3[J]. Applied Catalysis B:Environmental, 2009, **93**(1): 194−204.

[41] XU H D, WANG Y, CAO Y, FANG Z T, LIN T, GONG M C, CHEN Y Q. Catalytic performance of acidic zirconium-based composite oxides monolithic catalyst on selective catalytic reduction of NOx with NH3[J]. Chemical Engineering Journal, 2014, **240**: 62−73.

[42] ARTURO M-A, JAVIER S, JOSÉ C C, XOSÉ S, ADOLFO A, RENATO C. NO reaction at surface oxygen vacancies generated in cerium oxide[J]. Journal of the Chemical Society, Faraday Transactions, 1995, **91**: 1679−1687.

[43] FAN Z Y, SHI J W, GAO C, GAO G, WANG B R, NIU C M. Rationally Designed Porous MnOx-FeOx Nanoneedles for Low-Temperature Selective Catalytic Reduction of NOx by NH3[J]. Acs Applied Materials & Interfaces, 2017, **9**(19): 16117−16127.

[44] MA S B, ZHAO X Y, LI Y S, ZHANG T R, YUAN F L, NIU X Y, ZHU Y J. Effect of W on the acidity and redox performance of the

Cu0.02Fe0.2WaTiOx (a = 0.01, 0.02, 0.03) catalysts for NH3-SCR of NO[J]. Applied Catalysis B:Environmental, 2019, **248**: 226−238.

[45] SHU Y, SUN H, QUAN X, CHEN S. Enhancement of Catalytic Activity Over the Iron-Modified Ce/TiO2 Catalyst for Selective Catalytic Reduction of NOx with Ammonia[J]. Journal of Physical Chemistry C, 2012, **116**(48): 25319−25327.

[46] WANG H M, NING P, ZHANG Y Q, MA Y P, WANG J F, WANG L Y, ZHANG Q L. Highly efficient WO3-FeOx catalysts synthesized using a novel solvent-free method for NH3-SCR[J]. Journal of Hazardous Materials, 2020, **388**: 121812.

[47] GAO C, SHI J W, FAN Z Y, WANG B R, WANG Y, He C, WANG X B, LI J, NIU C M. "Fast SCR" reaction over Sm-modified MnOx-TiO2 for promoting reduction of NOx with NH3[J]. Applied Catalysis a-General, 2018, **564**: 102−112.

[48] GUI K T, LIANG H, ZHA X B. DRIFTS study of gamma Fe2O3 nano-catalyst for low-temperature selective catalyic reduction of NOx with NH3[J]. The Canadian Journal of Chemical Engineering, 2016, **94**(9): 1668−1675.

Fe_2O_3 对 $ZrTiO_4$ 载体 NH_3-SCR 催化性能的影响

袁龙腾[1,3]，胡　平[1,2,3,*]，胡卜亮[1,2,*]，韩嘉彧[1,2]，马升捷[1,3]，杨　帆[1,2]，AlexA. Volinsky[4]

（1. 西安建筑科技大学 材料加工国家与地方联合工程研究功能中心, 陕西 西安 710055;

2. 西安建筑科技大学冶金工程学院, 陕西 西安 710055;

3. 西安建筑科技大学机电工程学院, 陕西 西安 710055;

4. 南佛罗里达大学机械工程系, 4202 E.Fowler Ave., ENG 030, Tampa, FL 33620, 美国）

摘　要: NH_3-SCR 催化剂主要用于工业生产和汽车尾气清洁, 本研究采用“共沉淀-浸渍法”制备了新型 α% $Fe_2O_3/ZrTiO_4$ (α=0、8、12、15) 催化剂。结果表明, α% $Fe_2O_3/ZrTiO_4$ 催化剂的最佳成分配比的 12% $Fe_2O_3/ZrTiO_4$ 催化剂在 250−400 ℃ 条件下 NO_x 转化率大于 80%, 在 300 ℃ 时 NO_x 转化率接近 100%, 并且 N_2 选择性在 200−450 ℃ 大于 90%。在 $ZrTiO_4$ 表面负载 Fe_2O_3 后, 催化剂的氧化还原性能、表面酸度和 $O_\beta/(O_\alpha+O_\beta)$ 比例都有所提高, 这不仅归因于 α% $Fe_2O_3/ZrTiO_4$ 催化剂具有一种多孔结构, 还归因于活性组分 Fe_2O_3 和载体 $ZrTiO_4$ 之间的电子相互作用。此外, 原位 DRIFTs 反应表明, 12% $Fe_2O_3/ZrTiO_4$ 催化剂的 NH_3-SCR 反应遵循 Eley-Rideal 机制。明确的反应机制有利于更深入的了解 SCR 过程中 NO_x 转化的反应过程。这项工作为未来 Fe 基 SCR 催化剂在中温范围内替代 V 基催化剂提供了可行的策略。

关键词: $Fe_2O_3/ZrTiO_4$ 催化剂; NH_3-SCR; 多孔; 反应机制

中图分类号: O643.36　　**文献标识码:** A